NUMERICAL RESOLUTION OF PULSATING DETONATION WAVES

P. Hwang, R. P. Fedkiw, B. Merriman, T. D. Aslam, A. R. Karagozian, and S. J. Osher

University of California, Los Angeles, CA 90095-1597

Corresponding Author:

Professor A. R. Karagozian

Department of Mechanical and Aerospace Engineering

46-147D Engineering IV, UCLA

Los Angeles, CA 90095-1597

Phone: (310) 825-5653; FAX: (310) 206-4830

E-mail: ark@seas.ucla.edu

Revision submitted to

Combustion Theory and Modeling

June, 2000

NUMERICAL RESOLUTION OF PULSATING DETONATION WAVES

P. Hwang [*] R. P. Fedkiw [†] B. Merriman [‡] T. D. Aslam [§] A. R. Karagozian [¶] and S. J. Osher [‖]

University of California, Los Angeles, CA 90095-1597

1 Abstract

The canonical problem of the one-dimensional, pulsating, overdriven detonation wave has been studied for over thirty years, not only for its phenomenological relation to the evolution of multidimensional detonation instabilities, but for its providing a robust, reactive, high speed flowfield with which to test numerical schemes. The present study examines this flowfield using high order, essentially non-oscillatory (ENO) schemes, systematically varying the level of resolution of the reaction zone, the size and retention of information in the computational domain, the initial conditions, and the order of the scheme. It is found that there can be profound differences in peak pressures as well as in the period of oscillation, not only for cases in which the reaction front is under-resolved, but for cases in which the computation is corrupted due to a too-small computational domain. Methods for estimating the required size of the computational domain to reduce costs while avoiding erroneous solutions are proposed and tested.

---

[*]Graduate Student, Department of Mechanical and Aerospace Engineering; email: peterh@seas.ucla.edu

[†]Associate Researcher, Department of Mathematics; currently Assistant Professor, Stanford University; email: fedkiw@cs.stanford.edu

[‡]Researcher, Department of Mathematics; email: barry@math.ucla.edu

[§]Member of the Research Staff, Group DX-1, Los Alamos National Laboratory; email: aslam@lanl.gov

[¶]Professor, Department of Mechanical and Aerospace Engineering; email: ark@seas.ucla.edu (author to whom correspondence should be sent)

[‖]Professor, Department of Mathematics; email: sjo@math.ucla.edu

2 Introduction

Detonation phenomena have been examined theoretically and computationally now for over a century, beginning with the representation of the one-dimensional propagating detonation front as a discontinuity according to Chapman-Jouget (CJ) theory [1–3]. The theory of Zel'dovich [4], von Neumann [5], and Doering [6], which has come to be known collectively as the ZND detonation model, represents the detonation as the confluence of a shock wave moving at the detonation speed D, followed by a chemical reaction zone of finite length. The release of chemical energy sustains the propagation of the detonation front. This relatively simple model, which represents the chemical reaction by a single forward rate process, is known to capture many, if not most, of the essential physical phenomena associated with detonations, and as such the model has been extended by a number of researchers to more complex detonation configurations over the years [7, 8]. While recent advances in computational power have greatly enhanced the ability to numerically simulate multidimensional detonation phenomena with complex reaction kinetics, it is the ZND detonation, and instabilities associated with this one-dimensional representation, that is most often used as the canonical problem against which numerical schemes are validated.

Instabilities associated with detonation waves, while first recognized experimentally [9], were seen to occur for the 1D ZND model by Erpenbeck via linear stability analysis [10, 11] and non-linear stability analysis [12] and by Fickett and Wood [13] using a numerical method based on the characteristic net. Such pulsating instabilities have since been explored theoretically [14–16] and computationally [14, 17, 18] for overdriven detonation waves. The overdrive factor, f, is a parameter that relates the speed (D) of a given detonation to the Chapman-Jouget or CJ velocity, D_{CJ}, which corresponds to the detonation speed producing sonic flow behind the wave. The CJ speed corresponds to the minimum propagation speed necessary to sustain a detonation reaction. The overdrive factor is then defined as

$$f \equiv \left(\frac{D}{D_{CJ}}\right)^2 \tag{1}$$

Overdriven detonations correspond to overdrive factors f exceeding unity. Linear stability

analyses [10, 11, 14] identify the stability boundaries for the overdriven detonation within the parameter space defined by the ZND model; the number of instability modes is seen to increase as f approaches unity, i.e., the CJ condition. Despite rather extensive numerical examination of this canonical 1D unsteady detonation problem (e.g., [14, 17, 18]), there is no widespread consensus on how best to resolve this (and hence, by extension, a more complex) reactive flowfield, in terms of the required degree of resolution of the reaction zone, the amount of information required to be captured in the computational domain, the effect of initial conditions, and the degree of accuracy of the numerical scheme that is required. Since this reaction model forms the basis on which a large number of multidimensional (steady and transient) simulations are founded, and because the 1D pulsating detonation is used so widely as a "test" problem for high resolution numerical schemes, it is critical to understand precisely what does and does not constitute an accurate resolution of this flowfield. The present study describes a systematic study of resolution of this flowfield using high order schemes in order to clarify these and other issues pertaining to detonation simulation.

3 Problem Formulation and Numerical Methodology

3.1 Governing Equations

The governing equations used to simulate the inviscid, one-dimensional propagation of a detonation wave with a single step, irreversible chemical reaction are shown below, representing conservation of mass, momentum, energy, and species.

$$\vec{U}_t + \vec{F}(\vec{U})_x = \vec{S}(\vec{U}) \tag{2}$$

where the vector containing conserved variables, $\vec{U}$, the flux vector, $\vec{F}$, and the vector containing source terms, $\vec{S}$, are, respectively,

$$\vec{U} = \begin{pmatrix} \rho \\ \rho u \\ E \\ \rho Y \end{pmatrix} \qquad \vec{F}(\vec{U}) = \begin{pmatrix} \rho u \\ \rho u^2 + p \\ (E+p)u \\ \rho u Y \end{pmatrix} \qquad S(\vec{U}) = \begin{pmatrix} 0 \\ 0 \\ 0 \\ -K\rho Y e^{-\left(\frac{T_i}{T}\right)} \end{pmatrix} \tag{3}$$

where E may be written

$$E = \frac{p}{\gamma - 1} + \frac{\rho u^2}{2} + \rho q Y \tag{4}$$

In the above relations the variables have been made dimensionless with respect to the uniform state ahead of the detonation front (the unburned state). Here ρ represents density, p is the static pressure, u is the velocity, and γ is the ratio of specific heats. q is a non-dimensional heat release parameter which characterizes the amount of energy released during the reaction, and T_i represents the activation energy. Y is the reactant mass fraction which varies from 0 to 1, while K is the reaction-rate multiplier, which sets the spatial and temporal scales in the problem. The equation of state for an ideal gas is used here, and the gas is assumed to be calorically perfect (γ= constant).

The present study focuses on solution of the governing equations for the specific problem of the overdriven detonation wave with overdrive factor $f = 1.6$, for the parameters $q = 50$, $\gamma = 1.2$, and $T_i = 50$, conditions which are known to generate a single instability mode according to linear stability analyses [10, 11, 14] and according to various numerical studies [14, 17, 18]. An alternative overdrive condition, $f = 1.5$, is also explored in a few limited cases here. Linear stability analysis suggests that there are two unstable modes generated for this lower overdrive, although numerical simulations indicate the dominance of a nonlinear, single mode, large amplitude pulsating instability for $f = 1.5$ [14].

The computational problem is initiated here via two alternative methods: 1) a propagating shock front, and 2) a propagating ZND detonation wave. Results showing the effects of the alternative initial conditions are presented in Section 4.3. For the first alternative set of initial conditions, the pressure, density, and velocity on either side of the propagating shock front are chosen to correspond to the 1D overdriven detonation. For the parameters listed above, simultaneous solution

of the Rankine-Hugoniot and Rayleigh line equations produces a CJ speed of $D_{CJ} = 6.8095$. For a specified overdrive of $f = 1.6$, for example, the initial shock speed is $D = 8.6134$. As an alternative initial condition, the more usual spatial profiles associated with the ZND detonation, with farfield conditions corresponding to the specified overdrive, are chosen. The initial pressure profile across the initial ZND detonation is shown, for example, in Figure 1, where the wave propagates to the right. As will be shown in Section 4.3, the initial conditions in the problem have relatively little influence on the eventual limit cycle behavior of the instability; initial transients die out fairly quickly.

A suitable spatial scale in the problem is one based on the "half reaction length", $L_{\frac{1}{2}}$, i.e., the distance behind the shock in which half the reactants are consumed. Given f, a suitable K, the reaction-rate multiplier shown in equation (3), can be specified to give a spatial unit based on $L_{\frac{1}{2}}$. As done in [17, 18], a K of 230.75 is used to specify the $L_{\frac{1}{2}}$ as a spatial unit for $f = 1.6$. $K = 303.31$ is used for the $f = 1.5$ case.

3.2 Numerical Methodology

The present study uses the Essentially Non-Oscillatory (ENO) method [19–22] for spatial interpolation of the system of governing equations. ENO methods constitute a class of high accuracy, shock capturing numerical schemes for hyperbolic systems of conservation laws, based on upwind biased differencing in local characteristic fields. It has high accuracy (third order or higher) in smooth regions of the flow, and captures the motion of unresolved steep gradients without introducing spurious oscillations. Hence ENO is particularly well suited for resolution of flowfields in which there are shocks or flame fronts. ENO uses an adaptive polynomial interpolation constructed on the basis of decisions to avoid steep gradients in the data. The polynomial is also biased to extrapolate data from the direction of information propagation (i.e., upwind) for physical consistency and stability. To ensure that shocks and other steep gradients in the flow are properly captured (i.e., move at the correct speed), a discrete conservative form of the equations is used with the interpolation method.

To avoid entropy-violating expansion shocks near sonic points, which is where characteristic ve-

locities change sign, high order dissipation is added in the present study via the Local Lax Friedrichs (LLF) scheme, which adds extra numerical viscosity throughout the computational domain at each time step. A variant on the LLF scheme, the Roe Fix (RF) scheme, only adds extra numerical viscosity when there is a sonic point locally, i.e., where the eigenvalues change signs. This scheme is also explored in the present study. Although the LLF scheme is twice as computationally expensive as the RF scheme, in general LLF should be used with ENO because it is more robust for difficult problems.

Once the numerical approximation of the spatial terms has been completed using the ENO method, the conservation equations (2) can be written in the form

$$\vec{U}_t = \vec{f}(\vec{U}) \tag{5}$$

A third order TVD (Total Variation Diminishing) Runge-Kutta method is then used for the time discretization, since the method has high accuracy and, more importantly, a large time step stability region which includes a segment of purely imaginary linear growth rates. This feature ensures that for a sufficiently small time step (according to the Courant-Friedrichs-Levy or CFL condition), the time discretization will not introduce instability to the result. While there are other time integration methods that are designed specifically to solve systems of equations with stiff source terms (e.g., VODE [23]) more efficiently, they are not particularly well suited to solving the non-reactive conservation equations. Since the current simulation only involves a single step reaction, use of the TVD Runge-Kutta method is preferred; the CFL condition in this case incorporates the source term to insure stability. In simulations resolving a more complex chemical reaction mechanism, of course, operator splitting with implementation of a stiff ODE solver such as VODE is usually preferred. Further details on the numerical methods used here may be found in [24].

Validation of the numerical methods used here has been performed in two ways: 1) via application to "test" problems with exact or known solutions, and 2) via grid resolution studies for the pulsating detonation as described in Sections 4.1 and 4.2. The three "test" problems in 1) include a non-reactive shock tube with an exact solution, the problem of two interacting shocks created by a double shock tube, and a shock wave interacting with a flowfield in which there is a spatially

oscillatory density field. Details on the results of the test problems are described in [24]. Different order ENO schemes were examined, and it was found that the third order ENO scheme showed significant improvements in resolution of fine scale density structures over the second order ENO scheme. Hence for the present problem, most results will be shown for third order ENO schemes, except as noted.

4 Results

Following previous studies and the methodology outlined in Section 3, the shock pressure behind the evolving detonation wave (formulated in Section 3.1) is evaluated for galloping phenomena. This is done by monitoring the *local* maximum pressure in the vicinity of the shock which is initiated. It is important that one does not look *globally* in the computational domain for a maximum pressure as done, for example, in [25], since a global search can cause an erroneously "clipped" peak pressure profile to be generated. During the computation of a galloping detonation, it is possible for the shock pressure to drop lower than pressures well behind the shock as a result of the galloping phenomena. If one searches for the maximum pressure globally, it is possible that the pressure of one of the peaks well behind the shock is recorded and mistaken for the shock pressure. This phenomenon is shown in Figures 2ab, which compares computations of pulsating detonations under the same conditions, with the same resolution of the reaction zone and computational domain, but with global and local pressure maxima plotted, respectively.

The following sections describe computational results for the effects of the size of the computational domain, the resolution of the reaction zone, the initial conditions, and the effects of different numerical schemes on simulation of the pulsating 1D detonation wave. Focus is placed on the overdrive $f = 1.6$, although domain size studies also explore effects of an alternative overdrive, $f = 1.5$, on the detonation evolution. The results shown in Sections 4.1, 4.2, and 4.3 correspond to the 3rd order ENO method with the Local Lax Friedrichs (LLF) scheme.

4.1 Computational Domain Size

One of the biggest challenges of simulating unstable overdriven detonations is the high degree of resolution required to resolve the instability. In order to resolve the reaction zone behind the propagating shock wave, a large computational domain is often needed. This is particularly true if a long-time solution is being sought. For a particular computation, one is tempted to keep only a limited number of grid points behind the shock or detonation wave, with the reasoning that the information well behind the wave either never catches up with, or does not affect, the wave during the computation. This is particularly tempting to do in long time studies since the computational cost involved in keeping a large domain behind the shock is high. In the present study, however, we demonstrate that one must be careful in making such a cost-conscious simplification, as this can lead to the generation of erroneous flow properties. Here, we define a convenient way of calculating the minimum number of points needed to be kept behind the detonation during a calculation for the flow properties not to be affected by truncation of computational domain.

The problems created by overzealous truncation of the computational domain in the numerical simulation of an overdriven 1D ZND detonation are shown in Figures 3 and 4. These results, computed for a 1D detonation propagating to the right with an overdrive of $f = 1.6$, show the shock pressure long time history. The domain space retained behind the propagating shock front consists of $10L_{\frac{1}{2}}$'s and $50L_{\frac{1}{2}}$'s, for Figures 3 and 4, respectively. Both computations have the same spatial grid resolution of 20 points per $L_{\frac{1}{2}}$ and the same initial conditions (that of the propagating shock); the only difference is in the size of the domain that is being computationally updated behind the detonation front. It is seen that the evolution of the peak pressure behind the shock exhibits very different behaviors, depending on the size of this computational domain space. In Fig. 3, the oscillatory peak pressure profile "fans" out with increasing time, suggesting that the galloping amplitude of the peak detonation pressure is increasing as the wave propagates. Yet in Fig. 4, it is seen that the oscillatory pressure profile "shrinks" with increasing time, suggesting that the galloping amplitude of the shock pressure is decreasing as the shock propagates. Phenomena such as this, where the computational results are sensitive to the size of the computational domain, are highly undesirable.

Differences in the long time histories shown in Figures 3 and 4 result from the fact that, as the shock propagates, flow properties behind the shock eventually catch up to the shock via $u + c$ waves which travel at a speed greater than D. If too small a domain space behind the shock is retained in the computation (e.g., 10 $L_{\frac{1}{2}}$'s in Figure 3), the points at the edge of the computational domain cease to be updated after a certain amount of time into the computation, which leads to a corruption of the data in that region. The $u + c$ waves emanating from the corrupted data eventually catch up with the shock itself, thus erroneously altering shock properties.

A simple way to prevent these phenomena from occurring, of course, is to include all spatial nodes behind the propagating detonation wave at all times in the computation. In this way, all nodes are being updated at each time step, and the correct information is always propagated to the shock front. Yet for studies in which the long term behavior of the shock is of interest, the computational cost of retaining a domain that includes all points behind the propagating shock can become prohibitively large. It is thus proposed that the size of the computational domain should be chosen so as to contain the *minimum* number of points that insure that no corrupted $u+c$ waves will be able to catch up with the shock within the computational time of interest.

Figure 5 shows on a nondimensionalized x-t diagram how, in a very approximate way, corrupted information can catch up to the propagating shock front. At the onset of the simulation, the shock (or ZND detonation) starts from $x = 0$ and propagates to the right at an approximate speed D into a computational domain of length L, which is given in units of the reaction half-length $L_{\frac{1}{2}}$. For an overdriven detonation with $f = 1.6$ and detonation speed $D \approx 8.6$, for example, simulations show that the speed of $u + c$ waves generally fluctuate initially between 10 and 11. Taking the more aggressive value of the initial $u + c$ wave as $u + c = A = 11$, this means the difference in speeds between the $u + c$ wave and the shock front is $A - D = 2.4$. At time $\frac{L}{D}$, then, the shock has traveled the distance of the computational domain, L, so that points, starting at $x = 0$, are eliminated or "thrown out" of the computation after this time. Successive points at the left end of the domain continue to be eliminated in time as the detonation front propagates to the right, so that the distance between the detonation and the left end of the domain is always L. The $u + c$ wave associated with the first point to be eliminated (at $s = 0$), presumably containing data that

have not been updated and thus are corrupted, eventually intercepts the shock as shown in Fig. 5. For $f = 1.6$, this interception occurs at time $T = \frac{L}{A-D} + \frac{L}{D} = \frac{L}{2.4} + \frac{L}{8.6}$ and at the location $x = \frac{AL}{A-D} = \frac{11L}{2.4}$. Hence in order to insure that the computation is correct, the "time to initiation of data corruption" T must be larger than the *desired* time to which a solution is required. In other words, the computation must be complete for the purpose of the study *before* the shock is affected by the first corrupted $u + c$ wave obtained from data points eliminated from the computational domain. Thus if a solution for the overdriven 1D detonation is sought which is valid up until nondimensional time T, the computational domain size L should be specified for the present case such that

$$T \leq \frac{L}{A-D} + \frac{L}{D} \Longrightarrow L \geq CT \tag{6}$$

where the constant $C \equiv \frac{D(A-D)}{A}$. Rough approximations for the parameters A, D, and C for 1D detonations with overdrives of $f = 1.5$ and 1.6, for example, are given in Table 1 below.

Overdrive f	D	A	C
1.6	8.6	11	1.88
1.5	8.34	12	2.54

Table 1. Approximate values of initial detonation speed D, initial $u + c$ wave speed A, and constant C for the two overdrives considered in the present study.

As an example, if one is interested in the solution for the overdriven detonation with $f = 1.6$ up until the nondimensional time $T = 40$, then from equation (6), $L \geq 75$, i.e., a computational domain of at least $L = 75$ reaction half-lengths should be retained behind the shock front in order to insure the accuracy of the computation. At the final solution time $T = 40$, at which the "corrupted" $u + c$ characteristic has caught up with the propagating detonation front, the front has traveled a total distance of approximately $x = 11L/2.4 = 344$ reaction half-lengths during the entire computation. At this time, however, the actual domain retained in the computation is only $L = 75$ in length, indicating that nearly 80% of the total possible domain has been eliminated from

the (still accurate) computation. This constitutes a substantial savings in computational cost over the simple procedure in which all nodes behind the shock (i.e., for a domain length of 344) are retained in the computation.

The analysis associated with equation (6) strictly holds for a steadily propagating detonation wave, of course, yet one can demonstrate that the real time-dependent solution has virtually the same properties. Results for a simulation of the $f = 1.6$ overdriven detonation, starting with a "propagating shock front" at the location $x = 75$, are shown in Figure 6. A 5th order ENO method is used here to calculate the shock/detonation location as a function of time; the motion of a single $u+c$ characteristic, emanating from $x = 0$ at time $t = 0$, is also computed and is shown in Figure 6. All information behind the shock front is kept in the computational domain. At a nondimensional time of about 40, the two wave fronts are observed to intersect. Since the wave fronts were initially 75 reaction half-lengths apart, this time of intersection of the waves is the same as the "time to corruption of data", T, predicted by the approximate theory, equation (6). The closeness of the computed intersection time ($T \approx 40$) to that prediced by equation (6) is remarkable. It is also noted that the shock/detonation front has actually traveled a distance in the computation (Figure 6) of about 342 reaction half-lengths, very close to the predicted distance of 344 reaction half-lengths noted previously for the approximate analysis.

Figures 7 to 11 and 12 to 14 exhibit a systematic study of the effects of computational domain size, for two different overdrives, $f = 1.6$ and 1.5, respectively. In both sets of computations, $T = 85$ is selected, and 20 grid elements per reaction half length $L_{\frac{1}{2}}$ are used in this section for detonation resolution. These computations allow a verification of the rough estimate for domain size from equation (6) to be made. For example, for an overdrive of $f = 1.6$, a computational domain of $L = 160$ reaction half-lengths is estimated from (6) to guarantee that no $u + c$ waves emanating from eliminated points will be able to catch up with the detonation. An "exact" solution is first obtained with a computation which retains every single node behind the propagating shock. Alternative computations are then performed for successively increasing domain sizes. Figure 7, for example, displays results for a computation with a domain length (behind the shock) of $L = 3L_{\frac{1}{2}}$ as compared with the "exact" solution. The shortened domain causes an erroneously stable shock

pressure profile to be predicted, and the first shock pressure peak is not even captured correctly. Figure 8 shows that, with a domain of $5L_{\frac{1}{2}}$, the first shock pressure peak is captured, thus providing an unstable shock pressure profile. Correctly capturing the first peak is clearly necessary even to begin to form the galloping phenomenon for the detonation. Yet the computational domain length (behind the shock) of $5L_{\frac{1}{2}}$ soon causes the results to deviate from the exact solution due to corruption by erroneous $u + c$ waves. Results with a computational domain of $10L_{\frac{1}{2}}$, shown in Figure 9, show agreement with the exact solution up to about the third peak. The overall profile is a significant improvement over the prior two cases, however. The agreement with the exact solution improves substantially as the computational domain size is increased to $50L_{\frac{1}{2}}$ and then to $75L_{\frac{1}{2}}$ (Figures 10 and 11, respectively), although the *period* of the pulsation in shock pressure converges less rapidly than does the peak pressure amplitude. At computational domain sizes of $150L_{\frac{1}{2}}$, no difference is observed between the results obtained and the exact solution, since the domain size here lies just below the completely accurate simulation according to the theory in equation (6).

Similar observations are made when the overdrive is reduced to $f = 1.5$, as shown in Figures 12 to 14. As observed by Bourlioux, *et al.* [14], while linear stability analysis suggests that there are two unstable modes generated at this lower overdrive, numerical simulations indicate the dominance of a single mode, large amplitude pulsating instability. As for the $f = 1.6$ case, the computation is closer to the "exact" solution when the domain size is closer to that predicted by equation (6) (domain size $L = 216$ for $T = 85$; see Table 1).

Table 2 provides a summary of how the computed results (e.g., as shown in Figures 7 to 11 and 12 to 14) compare with those estimated from the approximation in equation (6). For example, for $f = 1.6$, equation (6) predicts that a computational domain of $L = 3$ (in units of $L_{\frac{1}{2}}$) will cause the initiation of a deviation from the "exact" solution to occur at a time $T = 3/1.88 = 1.6$. As a comparison, the time at which the computed solution with $L = 3$ actually deviates from the "exact" solution is $T = 2.5$, meaning that the computation is corrupted *later* than estimated by (6). This "deviation" from the "exact" result is determined by evaluating the nondimensional time at which the peak pressure in the computation with the shortened domain begins to deviate (by a prescribed percentage) from the peak pressure computed using the "exact" solution, in which all

nodes behind the shock are retained.

Domain Size $\left(L_{\frac{1}{2}}\right)$	Time T to Deviation from "Exact" Solution			
	$f = 1.6$ (est., eqn. (6))	$f = 1.6$ (observed)	$f = 1.5$ (est., eqn. (6))	$f = 1.5$ (observed)
3	1.6	2.5	1.2	2
5	2.7	8	2.0	8
10	5.3	19	3.9	18
50	26.6	55	19.7	54
75	39.9	78	29.5	76

Table 2. Estimated and observed (from computations) time of data corruption for the two overdrives considered, for various computational domain sizes.

Table 2 suggests that the rough estimate in equation (6) is actually overly conservative, since the results obtained using a given computational domain appear to break down well *after* the time predicted by the equation. This is likely due to the fact that the corruption of the shock data does not instantaneously manifest itself but rather takes a certain amount of time to build up before manifestation. Equation (6) merely estimates the time when the first $u + c$ wave catches up with the shock; this estimate is actually quite accurate, as demonstrated in Figure 6. But the estimate does not take into account the *extent* of corruption of the shock data (by multiple "erroneous" $u + c$ waves) that is required to cause enough damage for the shock data to be visible. Hence equation (6) can be used with confidence to be able to *conservatively estimate*, a priori, the size of the computational domain that is required to generate an accurate (and computationally much less expensive) solution at the desired time.

4.2 Reaction Zone Resolution

There has been some debate in recent numerical studies of detonation phenomena as to how many grid points per reaction half-length, $L_{\frac{1}{2}}$, are required to fully resolve the detonation structure. There have been suggestions that as many as 20 points per $L_{\frac{1}{2}}$ are required [14, 17], while other

studies have suggested 10, or even 5 points per $L_{\frac{1}{2}}$ are sufficient for accurate resolution [25]. Here, a systematic study using the 3rd order ENO method with LLF and with different spatial grid resolution (numbers of grid points per $L_{\frac{1}{2}}$) is presented. Computations are done here for an overdrive of $f = 1.6$, up to nondimensional time $t = 40$, sufficient to observe how the spatial grid size affects the shock pressure results. The computational domain length behind the propagating shock that is used here is calculated from the conservative estimate in equation (6), hence data corruption does not occur due to a shortened computational domain. Results are presented as Figures 15 to 18. For all cases, a baseline spatial grid size of 80 points per $L_{\frac{1}{2}}$ is used to provide an essentially "exact" solution for comparison.

Figure 15 provides the results of the computation with 5 points per $L_{\frac{1}{2}}$. The pressure peak amplitudes are generally seen to be more than 10% lower than those given by the "exact" or baseline solution, with an overprediction of shock pressure minimum as well. The period of the oscillation is also seen to be quite different from that of the baseline mesh. The results of the computation with 10 points per $L_{\frac{1}{2}}$ are shown in Fig. 16, and it is seen that a large improvement in pressure amplitude is obtained with this finer spatial grid size, although there remain large errors in pressure peak amplitude for the earlier peaks. The erroneous period of the oscillation remains the obvious sign that convergence has not occurred with this level of reaction zone resolution when compared to the baseline mesh. The computation done with 20 points per $L_{\frac{1}{2}}$ shows significant improvements over the previous two cases, as evident in Fig. 17. The pressure peak amplitudes have almost converged, and the galloping period deviates from that of the baseline mesh by only a few percent. When the reaction zone is resolved by 40 points per $L_{\frac{1}{2}}$, both pressure peak amplitude and galloping period are much closer to the baseline result.

Although obvious improvements were seen when the spatial grid resolution increased, it is difficult to determine *a priori* an optimal spatial grid resolution. From Figures 15 and 16, it is clear that 5 and 10 points per $L_{\frac{1}{2}}$ are not adequate to capture the detonation correctly for these standard overdriven detonation conditions. Even with 10 points per $L_{\frac{1}{2}}$, the errors in shock pressure peak amplitude (for the first two peaks) and galloping period are large enough that it may be concluded with confidence that the solutions have not converged. The choice between using 20 points per

$L_{\frac{1}{2}}$ and 40 points per $L_{\frac{1}{2}}$ is a more difficult one to make. Clearly the results obtained using 40 points per $L_{\frac{1}{2}}$ are superior to those obtained using 20 points per $L_{\frac{1}{2}}$, yet while the pressure peak amplitudes have almost converged with 20 points per $L_{\frac{1}{2}}$, it is the period that shows the major benefit of using 40 points per $L_{\frac{1}{2}}$. In fact there is still a visible phase difference between the results at 40 and at 80 points per $L_{\frac{1}{2}}$. The choice of which resolution to use will ultimately depend on the objective of the study being carried out, and how important computational cost is. The only real conclusion that may be drawn here is that 20 points per $L_{\frac{1}{2}}$ should be the *minimum* resolution used to study the overdriven detonation with single step kinetics.

4.3 Effects of Initial Conditions

As previously noted, initial conditions for both a propagating shock (with upstream and downstream conditions corresponding to the overdriven detonation) and a ZND detonation have been explored in the present study. Sample results showing the temporal evolution of peak pressure behind the propagating detonation wave for the ZND detonation as initial condition are shown in Figures 19 and 20, for resolutions of 10 and 40 grid points per $L_{\frac{1}{2}}$, respectively. These results may be compared with Figures 16 and 18, respectively, for the shock tube as initial condition. While the initial evolution of pressure obviously differs between the two sets of results, since initial conditions are the only parameters which are different, the plots are very closely matched in relative "time" after the third peak of the oscillation. It is seen that, even for an under-resolved propagating detonation (10 grid points per $L_{\frac{1}{2}}$, Figures 16 and 19), the initial conditions have relatively little effect on the computed pressure peak and the period of oscillation once 2-3 oscillations have been generated. These results are further quantified and compared in the following section.

4.4 Comparison Among Numerical Schemes

To this point, all results shown (except in Figure 6) have been obtained using third order ENO schemes, which are seen to be able to capture the galloping phenomena of the one-dimensional detonations considered here quite well. There are many other schemes used by other researchers, however, that have been documented in the literature for the overdriven detonation with $f = 1.6$

and with other parameters chosen as in the present set of computations, e.g., [14, 17, 18]. In addition, as mentioned in Section 3.2, ENO can be conveniently programmed to be n^{th} order in accuracy. Figure 21 shows how several schemes used in other studies compare with the present ENO schemes. Plotted are peak pressure magnitude behind the overdriven detonation (after reaching limit cycle-like pulsations) as a function of relative mesh spacing, where a relative mesh spacing of 1.0 corresponds to 10 points per $L_{\frac{1}{2}}$, a mesh spacing of 0.5 corresponds to 20 points per $L_{\frac{1}{2}}$, etc. The alternative schemes shown are the piecewise parabolic method (PPM) used by Bourlioux, et al [14], the Superbee limiter and Minmod limiter examined by Quirk [18], and the recent unsplit scheme of Papalexandris, et al. [17]. Results for both second order ENO ("ENO2") and third order ENO ("ENO3") methods are shown, with both Local Lax Friedrichs (LLF) and Roe Fix (RF) schemes. Results for the initial conditions of both the ZND detonation (marked "ZND") and the propagating shock (all other ENO results) are also given.

Nearly all schemes approach the correct peak pressure (at approximately $p \approx 99$, predicted in [13]) for very fine resolution of the reaction zone or a small value of the relative mesh spacing. Yet the third order ENO schemes, both with LLF and with RF, are able to achieve the correct peak pressure with a relatively coarse resolution (relative mesh spacing of 1.0). As noted in Section 4.3, the initial condition of the ZND detonation yields a solution for peak pressure that is nearly identical to that using the propagating shock (with a 0.5% difference in peak pressure at the coarsest grid resolution). In fact, with a relative mesh spacing of 0.5, or 20 points per $L_{\frac{1}{2}}$, all of the ENO schemes (second and third order) have essentially convergence in peak pressure, which is not true for most of the other schemes.

Yet as noted in Section 4.2, the converged value of the peak pressure does not tell the whole story with respect to an accurate resolution of this canonical problem. In Figure 22 the periods of pressure oscillation obtained by the different ENO schemes are compared, again, with inclusion of cases with the ZND detonation as the initial condition. Here, "period" is defined as the time between successive pressure peaks during the limit cycle oscillatory behavior of the detonation. In the present computations, the average time between the 3rd and 4th peak and the 4th and 5th peak is used to define "period"; these two times are always within 1% of each other for the computations

performed here.

The differences between the second order and third order ENO schemes are more apparent when one considers the period of oscillation. The third order schemes are clearly able to predict the period more accurately for a given mesh spacing than can the second order schemes. Yet all schemes converge to a period in the range 7.33 to 7.37 for a relative grid spacing below 0.2 (or more than 50 points per $L_{\frac{1}{2}}$). It should be noted that the nonlinear stability analysis for the $f = 1.6$ detonation by Erpenbeck [12] predicts periods of oscillation of 7.41 or 7.49, depending on the perturbation method used.

Figures 21 and Figure 22 suggest that it is not adequate, for signs of convergence, to look at peak pressure amplitude *alone* in validating an overdriven detonation computation. As shown in these figures, a mesh spacing which gives convergence in peak pressure amplitude may not give convergence in the period of oscillation. It is thus suggested that the more demanding criterion of convergence in oscillation period should be used, *in addition to peak pressure*, in validating numerical schemes being tested using the 1D overdriven detonation problem.

5 Conclusions

The canonical problem of the one-dimensional, pulsating, overdriven detonation wave with single step reaction kinetics has been studied here numerically using high order resolution ENO schemes. A systematic study of the effects of computational domain size, reaction zone resolution, initial conditions, and numerical methodology on detonation wave behavior is performed. Accuracy in the resolution of the overdriven detonation is found to be required both in terms of the magnitude of the peak pressure behind the wave as well as in the period of oscillation in the wave. It is found that, contrary to several published sets of results, a reaction zone resolution of at least 20 points per reaction zone half length $L_{\frac{1}{2}}$ is required for accurate resolution of the detonation wave with an overdrive of $f = 1.6$. Moreover, it is found that the selected computational domain size can have a significant effect on the accuracy of the computation. An approximate method for estimating the required computational domain size, based on the time to which an accurate solution is required, is

described in this study; this estimate may be used in predicting required computational domain size a priori, and can result in substantial computational savings. Initial conditions in the computation (the propagating ZND detonation vs. the propagating shock wave), when selected appropriately, are seen to yield essentially the same results for limit cycle behavior of the pulsating detonation. Finally, it is demonstrated that third order ENO methods, either with LLF or RF schemes, are able to resolve both peak pressures and periods of oscillations very accurately, with coarser spatial resolution than is required in other schemes.

6 Acknowledgements

This work has been supported at UCLA by the Office of Naval Research under Grants N00014-97-1-0027 and N00014-97-1-0968, with Dr. Wen Masters as technical monitor, and by NASA Dryden Flight Research Center under Grant NCC-2-374, with Dr. Stephen Corda as technical monitor. Dr. T. D. Aslam's work at Los Alamos National Laboratory was performed under the auspices of the United States Department of Energy.

7 References

References

[1] Chapman, D.L., "On the Rate of Explosion in Gases", *Philos. Mag.*, Vol. 47, 1899, pp. 90-104.

[2] Jouget, E., "On the Propagation of Chemical Reactions in Gases", *J. de Mathematiques Pures et Appliquees*, Vol. 1, 1905, pp. 347-425, continued in Vol. 2, 1906, pp. 5-85.

[3] Jouget, E., "Mecanique des explosifs", *Paris: Octave Doin et Fils*, 1917.

[4] Zel'dovich, Ia, B., "On the Theory of the Propagation of Detonation in Gaseous Systems", *Zh. Eksp. Teor. Fiz.*, Vol. 10, 1940, pp. 542-568.

[5] von Neumann, J., "Theory of Detonation Waves", *John Von Neumann, Collected Works*, Vol. 6, 1942.

[6] Doering, W., "On Detonation Processes in Gases", *Ann. Phys.*, Vol. 43, 1943, pp. 421-436.

[7] Bourlioux, A., Majda, A.J., "Theoretical and Numerical Structure for Unstable Two-Dimensional Detonations", *Combustion and Flame*, Vol. 90, 1992, pp. 211-229.

[8] Williams, D. N., Bauwens, L, and Oran, E. S., "Detailed Structure and Propagation of Three-Dimensional Detonations", *Twenty-Sixth Symposium (Int.) on Combustion*, 1996, pp. 2991-2998.

[9] Campbell, C., Woodhead, D.W., "The Ignition of Gases by an Explosion Wave. Part I. Carbon Monoxide and Hydrogen Mixtures", *J. Chem. Soc.*, 1927, pp. 1572-1578.

[10] Erpenbeck, J.J., "Stability of Steady-State Equilibrium Detonations", *Physics of Fluids*, Vol. 5, 1962, pp. 604-614.

[11] Erpenbeck, J.J., "Stability of Idealized One-Reaction Detonations", *Physics of Fluids*, Vol. 7, 1964, pp. 684-696.

[12] Erpenbeck, J.J., "Nonlinear Theory of Unstable One-Dimensional Detonations", *Physics of Fluids*, Vol. 10, 1967, pp. 274-288.

[13] Fickett, W., Wood, W.W., "Flow Calculations for Pulsating One-Dimensional Detonations", *Physics of Fluids*, Vol. 9, 1966, pp. 903-916.

[14] Bourlioux, A., Majda, A.J., Roytburd, V., "Theoretical and Numerical Structure for Unstable One-Dimensional Detonations", *SIAM Journal of Applied Mathematics*, Vol. 51, 1991, pp. 303-343.

[15] Lee, H.I., Stewart, D.S., "Calculation of Linear Detonation Stability: One-Dimensional Instability of Plane Detonation", *Journal of Fluid Mechanics*, Vol. 216, 1990, pp. 103-132.

[16] Clavin, P., He, L., "Stability and Nonlinear Dynamics of One-Dimensional Overdriven Detonations in Gases", *Journal of Fluid Mechanics*, Vol. 306, 1996, pp. 353-378.

[17] Papalexandris, M.V., Leonard, A., Dimotakis, P.E., "Unsplit Schemes for Hyperbolic Conservation Laws with Source Terms in One Space Dimension", *Journal of Computational Physics*, Vol. 134, 1997, pp. 31-61.

[18] Quirk, J.J., "Godunov-Type Schemes Applied to Detonation Flows", *Combustion in High-Speed Flows*, 1994, pp. 575-596.

[19] Harten, A., Osher S. J., Engquist, B. E., and Chakravarthy, S. R., "Some Results on Uniformly High-Order Accurate Essentially Nonoscillatory Schemes", *J. Appl. Numer. Math.*, Vol. 2, 347-377, 1986.

[20] Shu, C.W. and Osher, S., "Efficient Implementation of Essentially Non-Oscillatory Shock Capturing Schemes II", *Journal of Computational Physics*, Vol. 83, 1989, pp. 32-78.

[21] Fedkiw, R.P., Merriman, B., Donat, R., and Osher, S., "The Penultimate Scheme for Systems of Conservation Laws: Finite Difference ENO with Marquina's Flux Splitting", *Progress in Numerical Solutions of Partial Differential Equations*, edited by M. Hafez, Arachon, France, July, 1998

[22] Fedkiw, R.P., Merriman, B., Osher, S., "High accuracy numerical methods for thermally perfect gas flows with chemistry", *Journal of Computational Physics*, Vol. 132, No. 2, pp 175-190, 1997.

[23] Brown, P. N., Byrne, G. D., and Hindmarsh, A. C. "VODE: A variable coefficient ODE solver", *SIAM J. Scientific Statistical Computing* 10, pp. 1038-1051, 1989.

[24] Hwang, P., "Simulations of One-Dimensional Pulsating Detonations with Different Levels of Numerical Resolution" *UCLA Engineering Report* ENG-00-212, December, 1998.

[25] Engquist, B., Sjogren, B., "Robust Difference Approximations of Stiff inviscid Detonation Waves", *UCLA CAM Report*, Vol. 91-03, 1991.

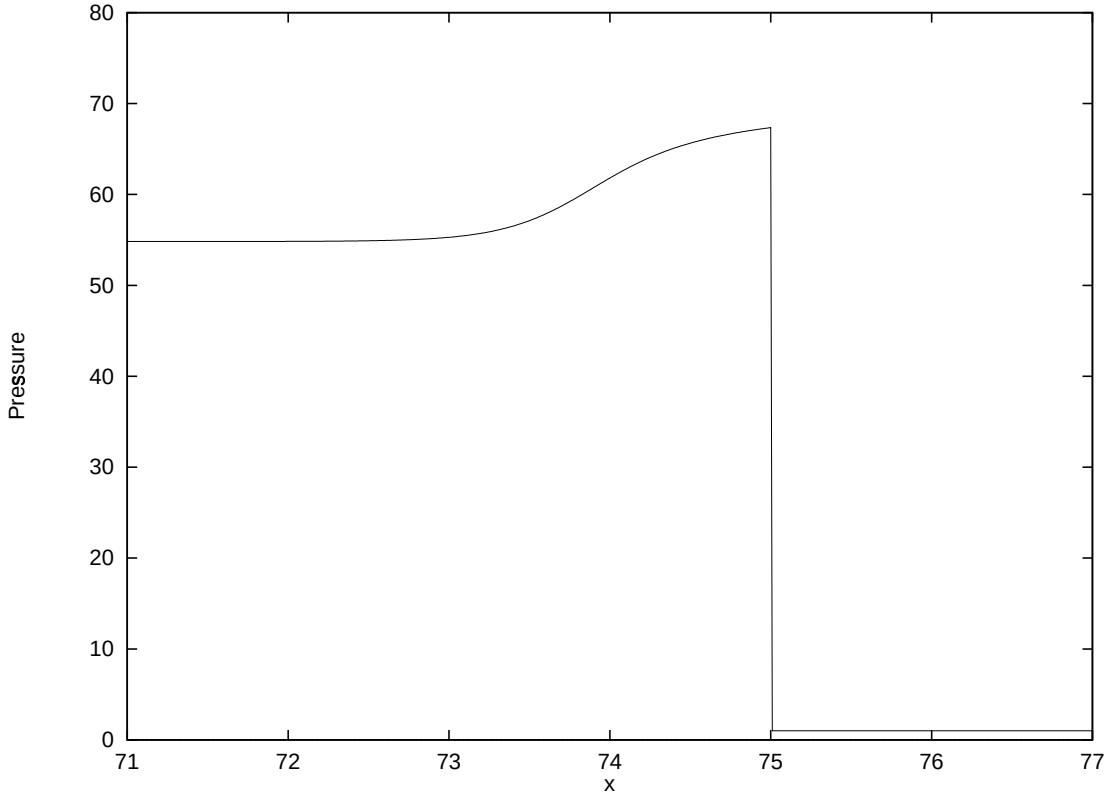

Figure 1: Spatial pressure distribution at computational time $t = 0$, for the initial condition representing the overdriven ZND detonation with $f = 1.6$.

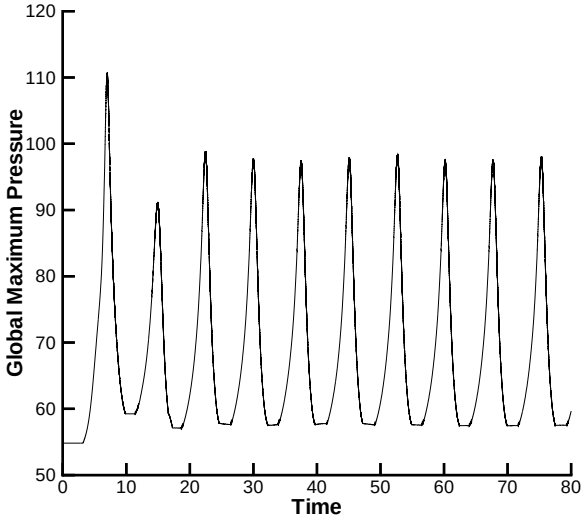

(a) Global pressure maxima

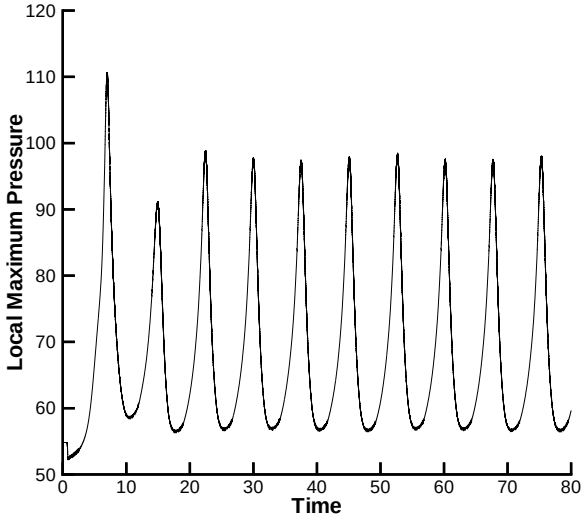

(b) Local pressure maxima

Figure 2: Plots of (a) the global pressure maxima and (b) the local pressure maxima (in the vicinity of the shock front) as a function of time. "Clipping" of the pressure profile occurs when global maxima are plotted.

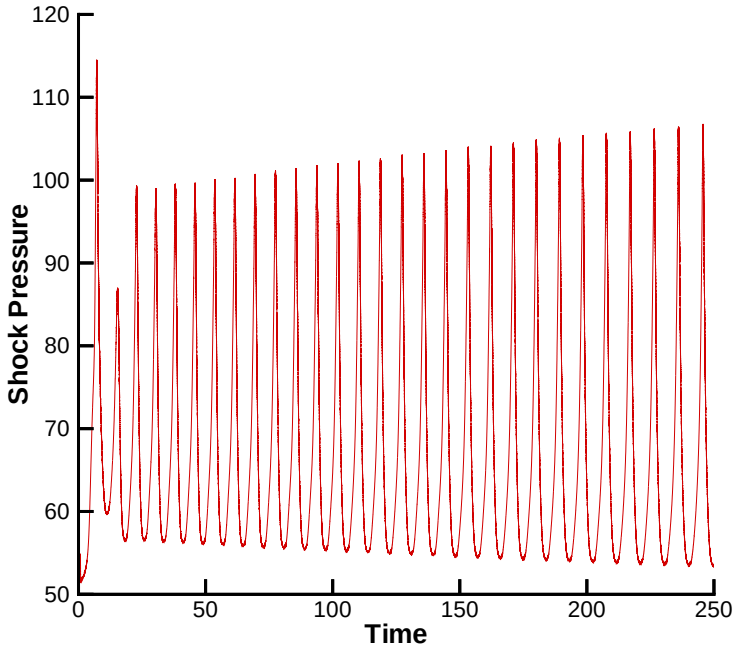

Figure 3: Pressure behind the shock front as a function of time for the overdriven detonation with $f = 1.6$, using 20 grid points per $L_{\frac{1}{2}}$, and with a computational domain size of $10L_{\frac{1}{2}}$'s. The initial conditions correspond to the propagating shock wave.

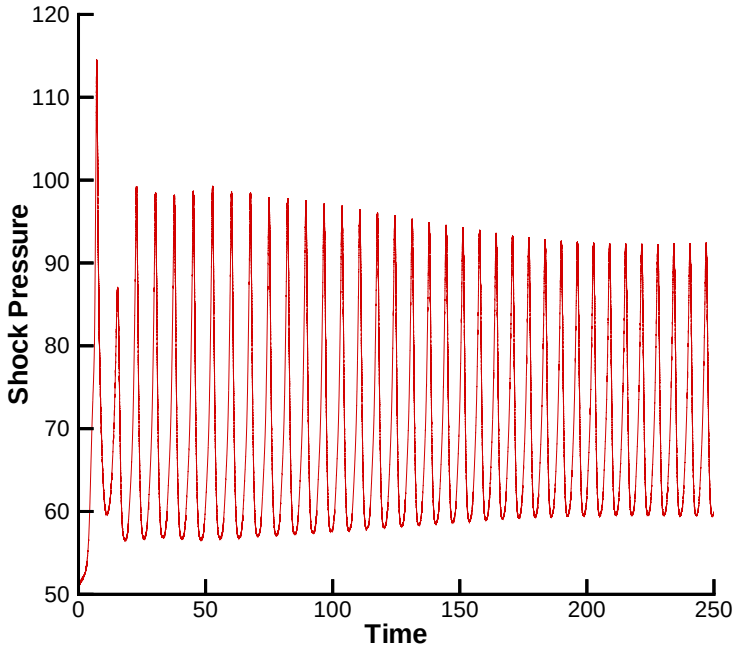

Figure 4: Pressure behind the shock front as a function of time for the overdriven detonation with $f = 1.6$, using 20 grid points per $L_{\frac{1}{2}}$, and with a computational domain size of $50L_{\frac{1}{2}}$'s. The initial conditions correspond to the propagating shock wave.

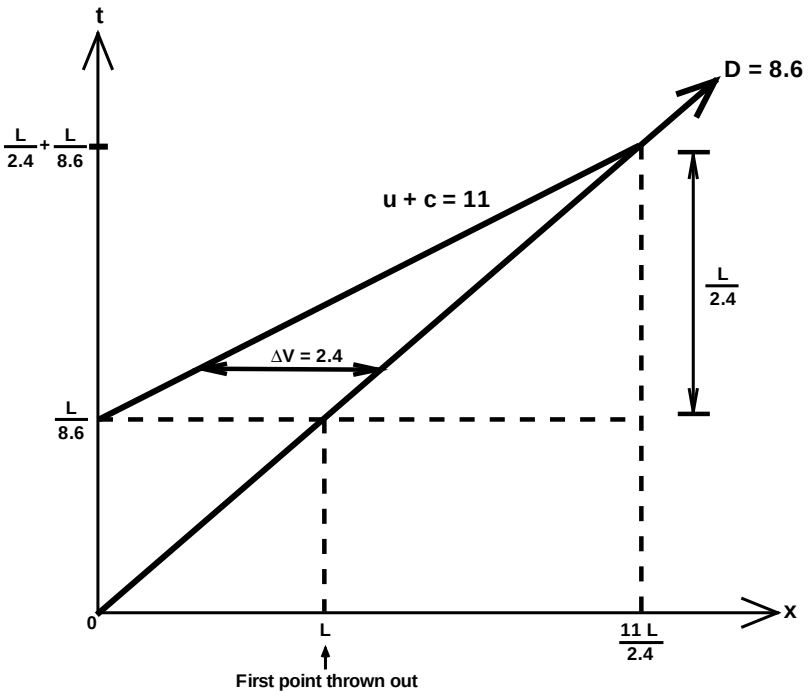

Figure 5: Non-dimensional $x - t$ diagram of the propagating shock front (speed $D = 8.6$) and the propagating $u + c$ wave (speed $u + c = 11$) which emanates from $x = 0$ at the time $L/8.6$ at which data have begun to be eliminated from the computational domain. Values here correspond to the overdrive $f = 1.6$.

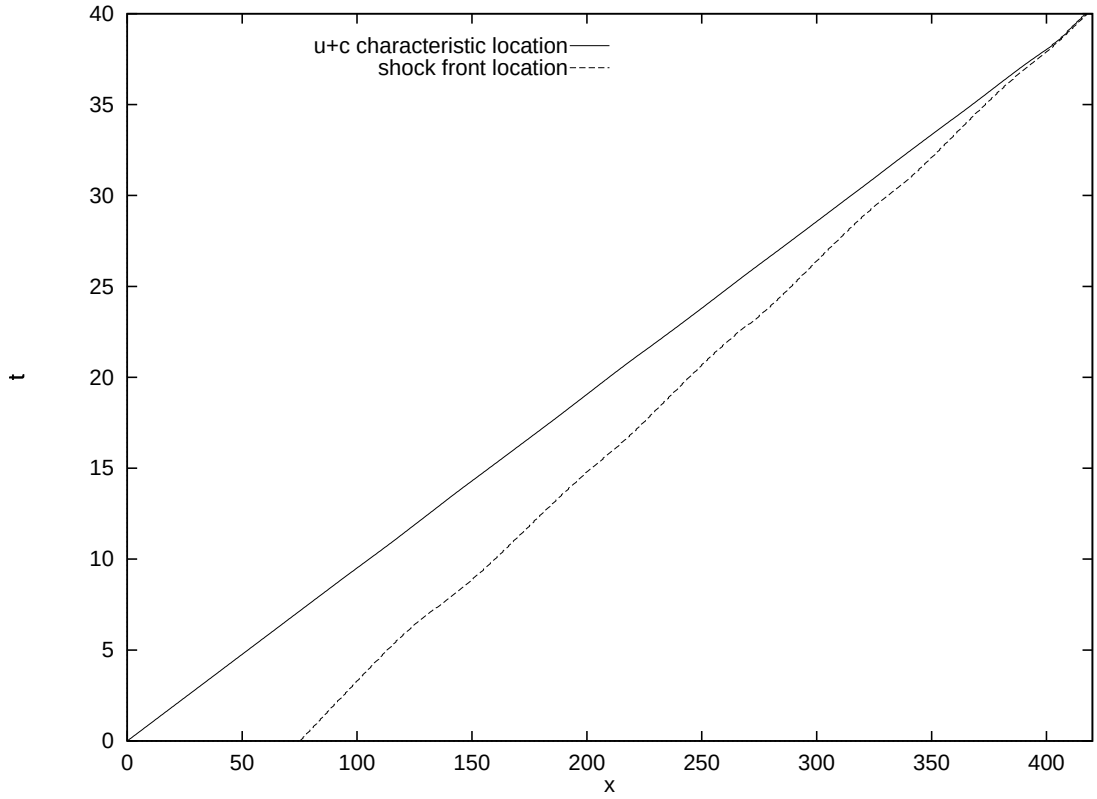

Figure 6: Non-dimensional $x-t$ diagram showing the propagating shock/detonation front (initiated at $x = 75$) and the actual propagating $u + c$ wave (emanating from $x = 0$), for the overdriven detonation with $f = 1.6$. The computation here uses a 5th order ENO scheme with 20 grid points per $L_{\frac{1}{2}}$ and with no elimination of data from the computational domain.

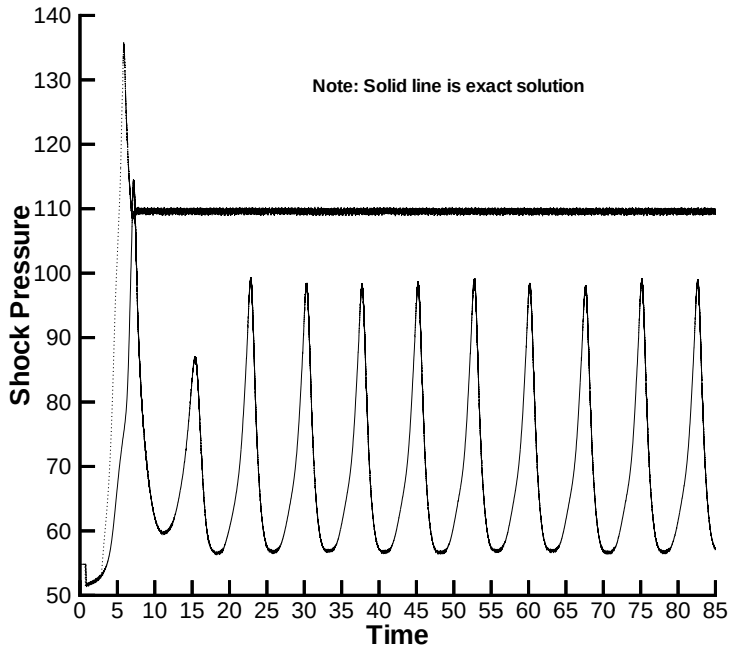

Figure 7: Pressure behind the shock front as a function of time for the overdriven detonation with $f = 1.6$, using 20 grid points per $L_{\frac{1}{2}}$, and with a computational domain size of $3L_{\frac{1}{2}}$'s. The 3rd order ENO method is used with the LLF scheme. Comparison is made with the "exact" solution, which retains every single node behind the shock. The initial conditions correspond to the propagating shock wave.

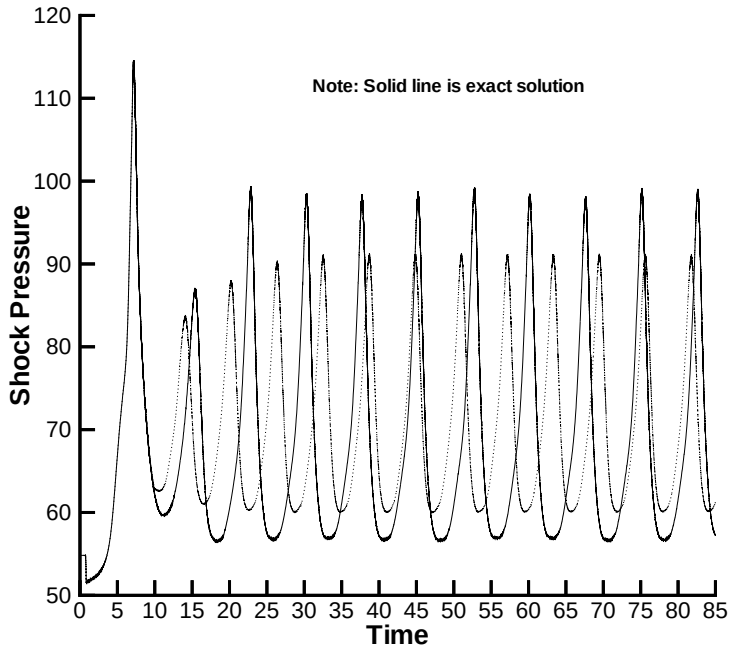

Figure 8: Pressure behind the shock front as a function of time for the overdriven detonation with f = 1.6, using 20 grid points per $L_{\frac{1}{2}}$, and with a computational domain size of $5L_{\frac{1}{2}}$'s. The 3rd order ENO method is used with the LLF scheme. Comparison is made with the "exact" solution, which retains every single node behind the shock. The initial conditions correspond to the propagating shock wave.

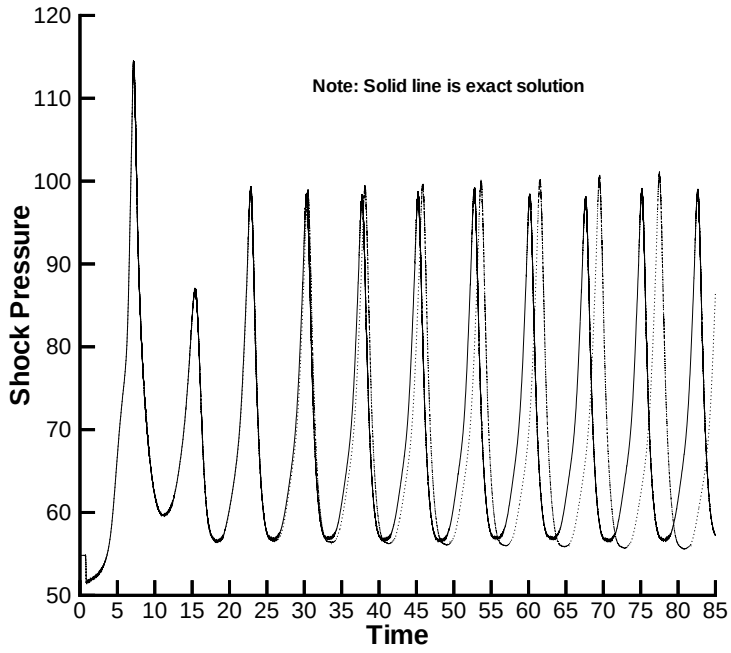

Figure 9: Pressure behind the shock front as a function of time for the overdriven detonation with f = 1.6, using 20 grid points per $L_{\frac{1}{2}}$, and with a computational domain size of $10L_{\frac{1}{2}}$'s. The 3rd order ENO method is used with the LLF scheme. Comparison is made with the "exact" solution, which retains every single node behind the shock. The initial conditions correspond to the propagating shock wave.

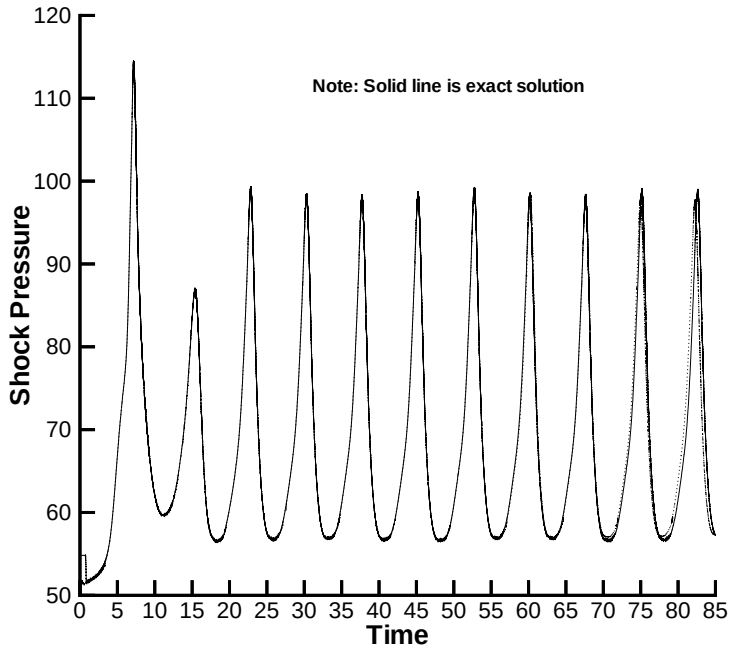

Figure 10: Pressure behind the shock front as a function of time for the overdriven detonation with $f = 1.6$, using 20 grid points per $L_{\frac{1}{2}}$, and with a computational domain size of $50L_{\frac{1}{2}}$'s. The 3rd order ENO method is used with the LLF scheme. Comparison is made with the "exact" solution, which retains every single node behind the shock. The initial conditions correspond to the propagating shock wave.

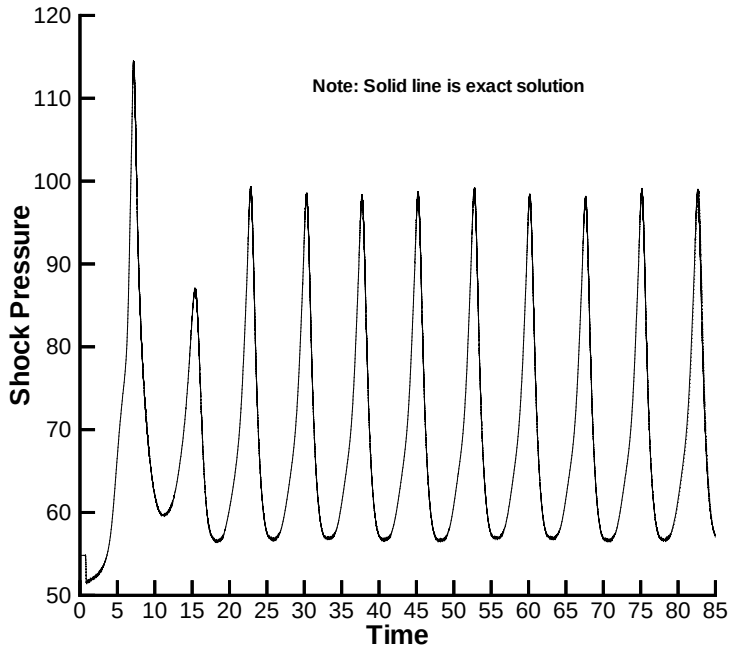

Figure 11: Pressure behind the shock front as a function of time for the overdriven detonation with $f = 1.6$, using 20 grid points per $L_{\frac{1}{2}}$, and with a computational domain size of $75 L_{\frac{1}{2}}$'s. The 3rd order ENO method is used with the LLF scheme. Comparison is made with the "exact" solution, which retains every single node behind the shock. The initial conditions correspond to the propagating shock wave.

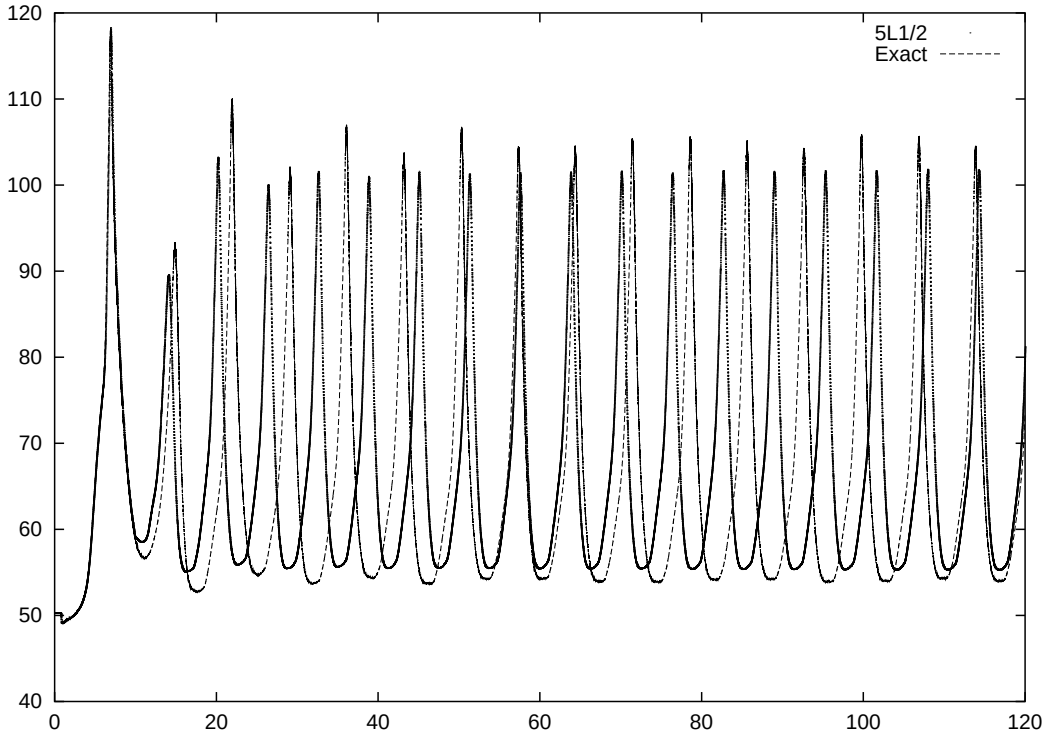

Figure 12: Pressure behind the shock front as a function of time for the overdriven detonation with $f = 1.5$, using 20 grid points per $L_{\frac{1}{2}}$, and with a computational domain size of $5L_{\frac{1}{2}}$'s. The 3rd order ENO method is used with the LLF scheme. Comparison is made with the "exact" solution, which retains every single node behind the shock. The initial conditions correspond to the propagating shock wave.

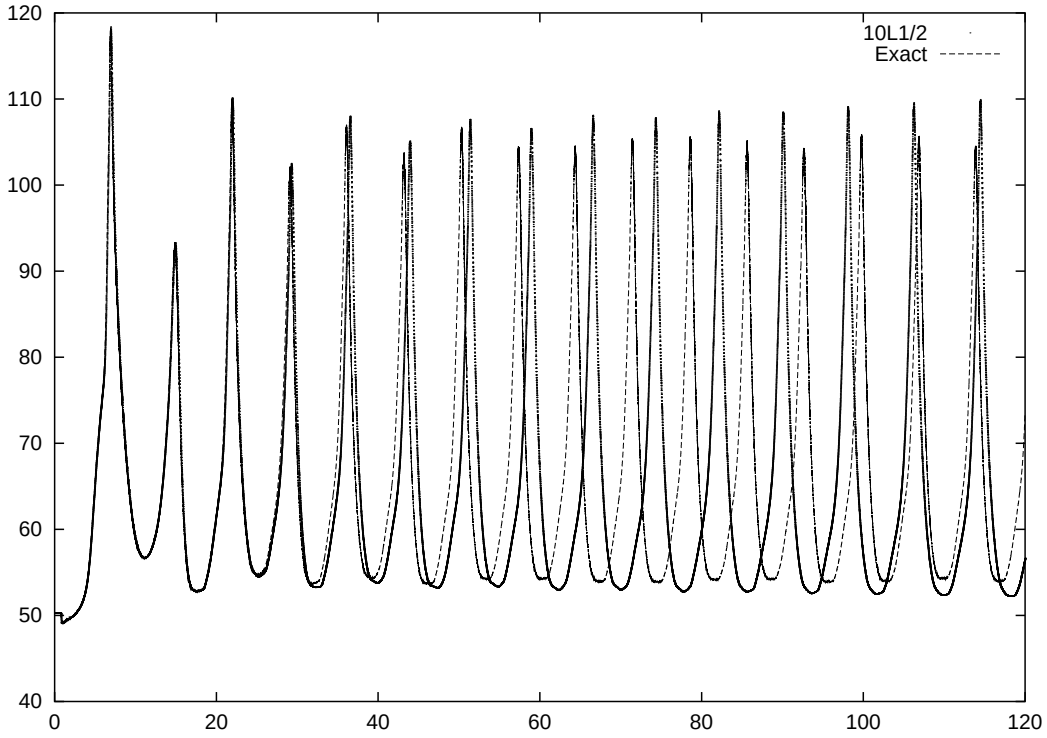

Figure 13: Pressure behind the shock front as a function of time for the overdriven detonation with $f = 1.5$, using 20 grid points per $L_{\frac{1}{2}}$, and with a computational domain size of $10L_{\frac{1}{2}}$'s. The 3rd order ENO method is used with the LLF scheme. Comparison is made with the "exact" solution, which retains every single node behind the shock. The initial conditions correspond to the propagating shock wave.

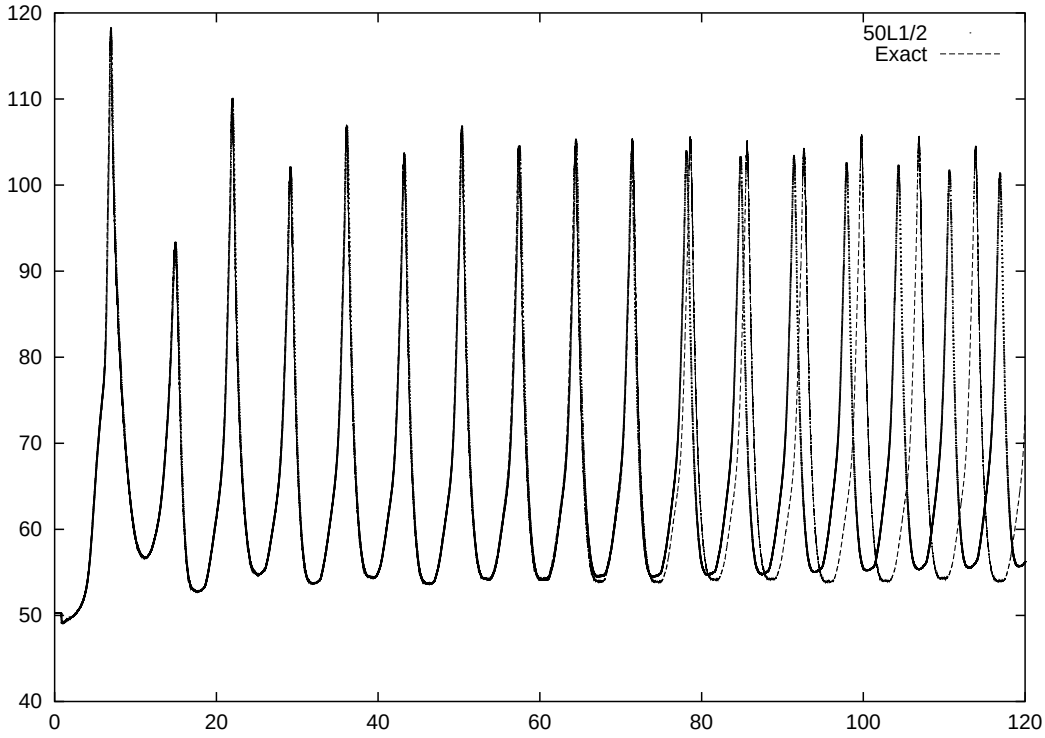

Figure 14: Pressure behind the shock front as a function of time for the overdriven detonation with $f = 1.5$, using 20 grid points per $L_{\frac{1}{2}}$, and with a computational domain size of $50L_{\frac{1}{2}}$'s. The 3rd order ENO method is used with the LLF scheme. Comparison is made with the "exact" solution, which retains every single node behind the shock. The initial conditions correspond to the propagating shock wave.

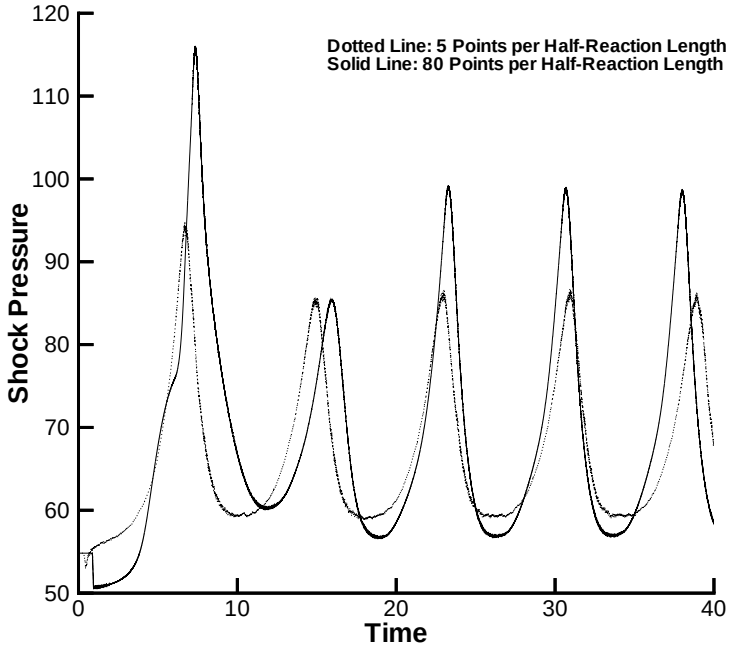

Figure 15: Pressure behind the shock front as a function of time for the overdriven detonation with $f = 1.6$, using 5 grid points per $L_{\frac{1}{2}}$, and with a computational domain size of $75L_{\frac{1}{2}}$'s. The 3rd order ENO method is used with the LLF scheme. Comparison is made with the baseline case where 80 grid points per $L_{\frac{1}{2}}$ is used. The initial conditions correspond to the propagating shock wave.

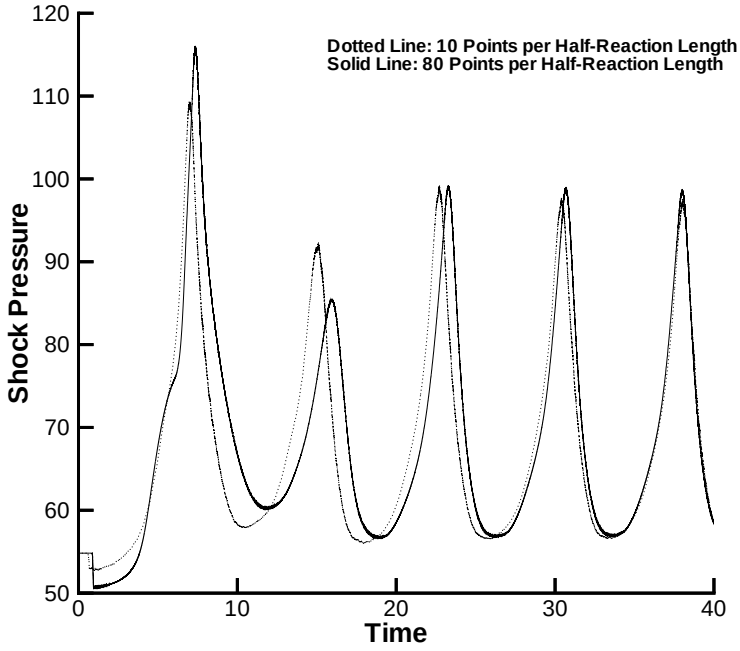

Figure 16: Pressure behind the shock front as a function of time for the overdriven detonation with $f = 1.6$, using 10 grid points per $L_{\frac{1}{2}}$, and with a computational domain size of $75L_{\frac{1}{2}}$'s. The 3rd order ENO method is used with the LLF scheme. Comparison is made with the baseline case where 80 grid points per $L_{\frac{1}{2}}$ is used. The initial conditions correspond to the propagating shock wave.

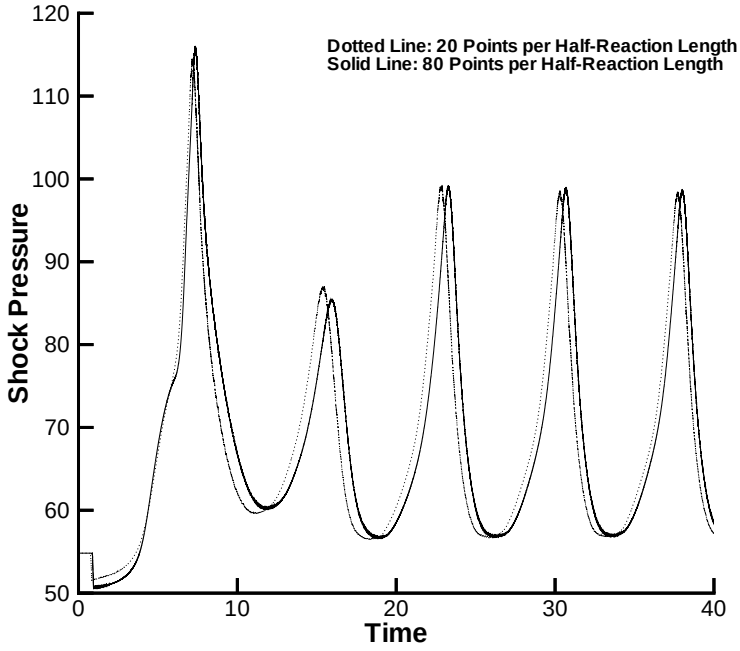

Figure 17: Pressure behind the shock front as a function of time for the overdriven detonation with $f = 1.6$, using 20 grid points per $L_{\frac{1}{2}}$, and with a computational domain size of $75L_{\frac{1}{2}}$'s. The 3rd order ENO method is used with the LLF scheme. Comparison is made with the baseline case where 80 grid points per $L_{\frac{1}{2}}$ is used. The initial conditions correspond to the propagating shock wave.

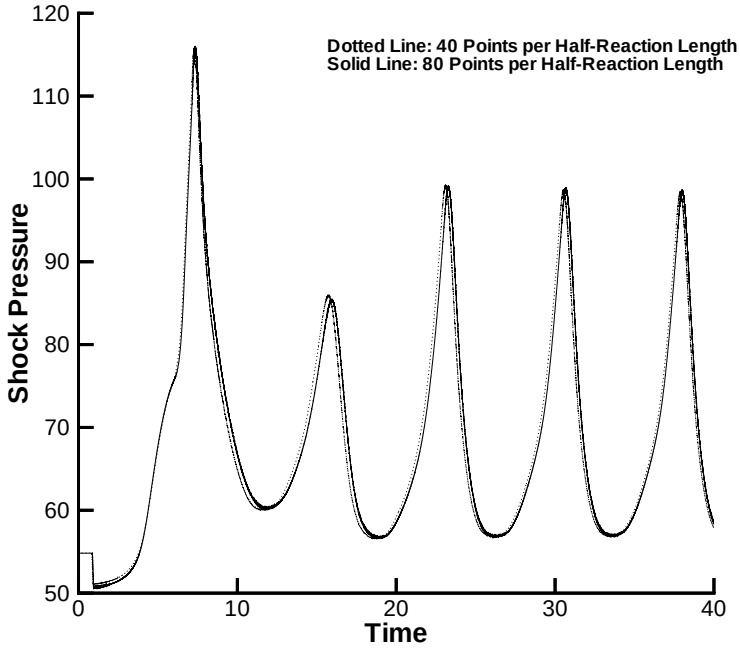

Figure 18: Pressure behind the shock front as a function of time for the overdriven detonation with $f = 1.6$, using 40 grid points per $L_{\frac{1}{2}}$, and with a computational domain size of $75L_{\frac{1}{2}}$'s. The 3rd order ENO method is used with the LLF scheme. Comparison is made with the baseline case where 80 grid points per $L_{\frac{1}{2}}$ is used. The initial conditions correspond to the propagating shock wave.

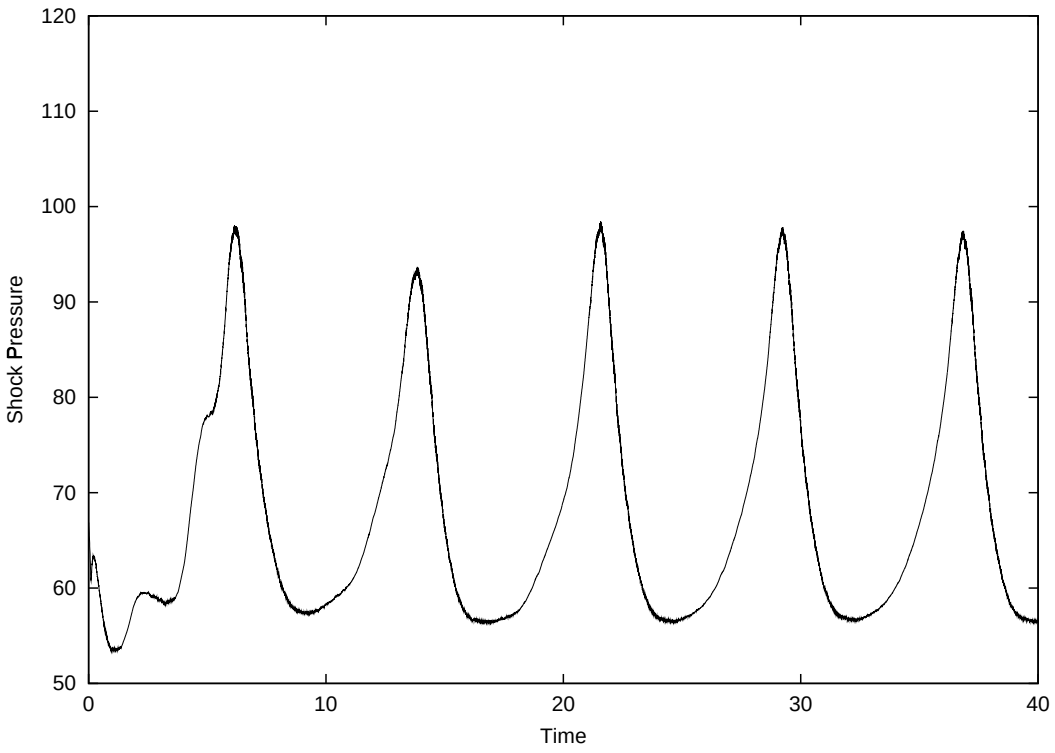

Figure 19: Pressure behind the shock front as a function of time for the overdriven detonation with $f = 1.6$, using 10 grid points per $L_{\frac{1}{2}}$, and with a computational domain size of $75L_{\frac{1}{2}}$'s. The 3rd order ENO method is used with the LLF scheme. The initial conditions correspond to the propagating ZND detonation (Figure 1).

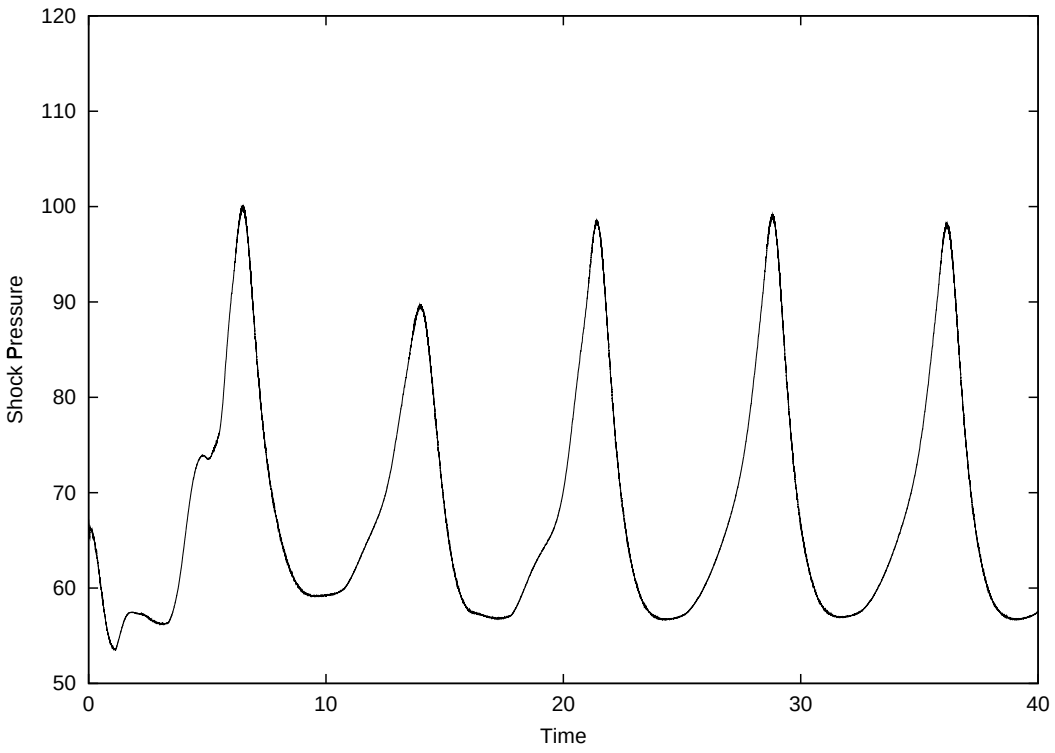

Figure 20: Pressure behind the shock front as a function of time for the overdriven detonation with $f = 1.6$, using 40 grid points per $L_{\frac{1}{2}}$, and with a computational domain size of $75L_{\frac{1}{2}}$'s. The 3rd order ENO method is used with the LLF scheme. The initial conditions correspond to the propagating ZND detonation (Figure 1).

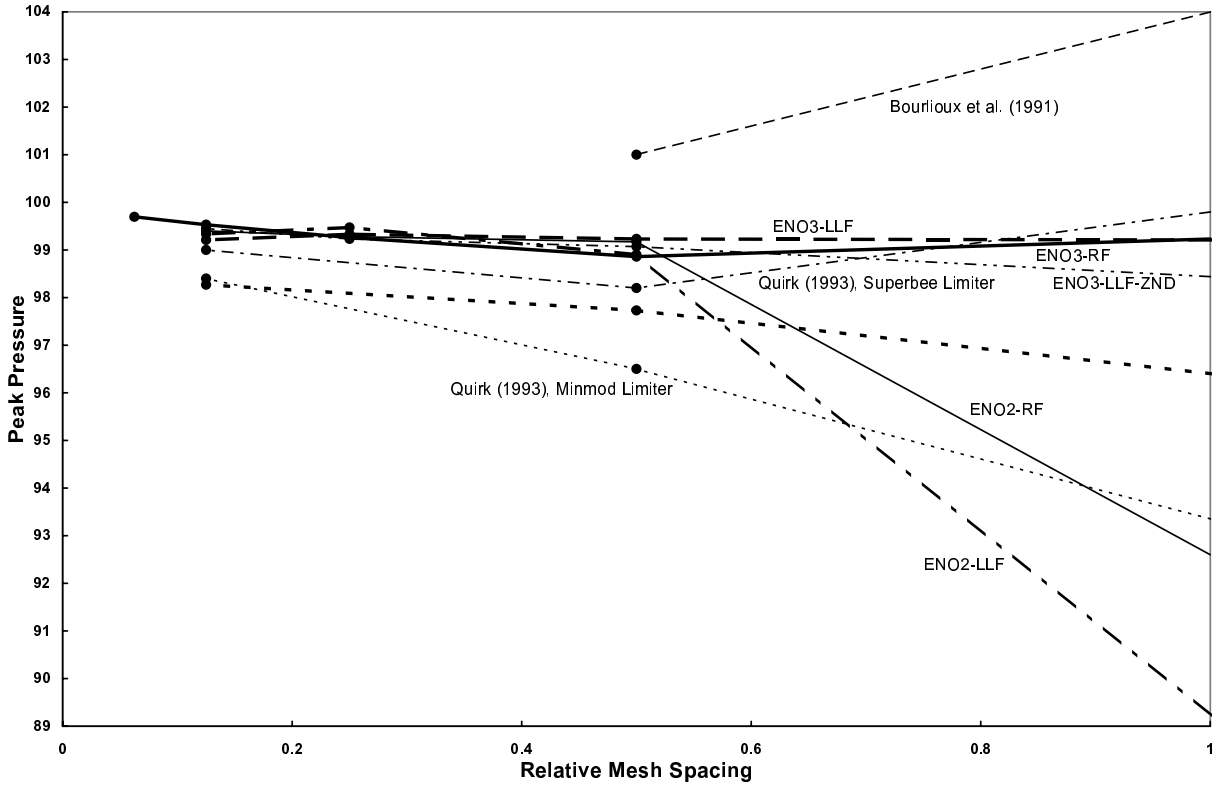

Figure 21: Peak pressure behind the shock front for the sustained pulsating detonation as a function of relative mesh spacing (= 10 / no. grid points per $L_{\frac{1}{2}}$), for $f = 1.6$. Comparison is made among numerical schemes used in prior studies and the present ENO schemes. The notation "ZND" refers to the ZND detonation as the initial condition; without this notation for ENO schemes, the initial conditions corresponds to the propagating shock.

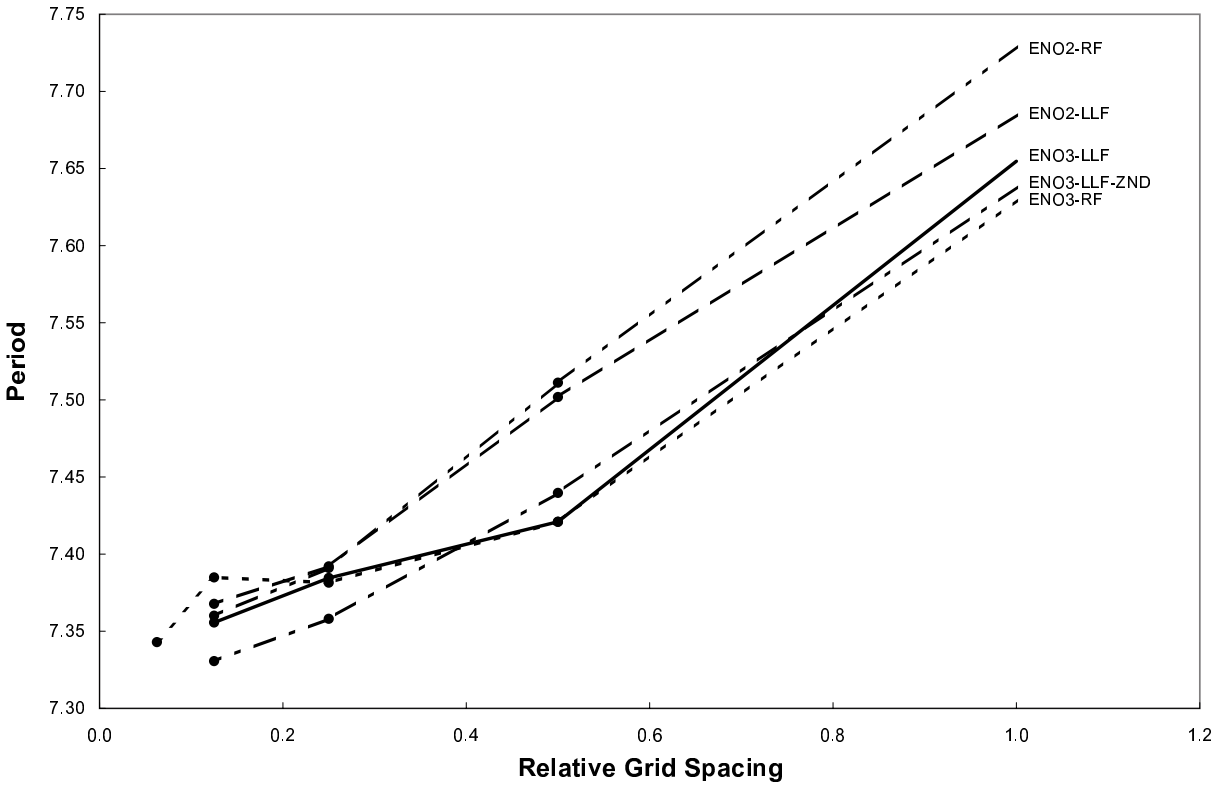

Figure 22: Period of time between successive pressure peaks for the pulsating detonation as a function of relative mesh spacing (= 10 / no. grid points per $L_{\frac{1}{2}}$), for $f = 1.6$. Comparison is made among the present ENO schemes. The notation "ZND" refers to the ZND detonation as the initial condition; without this notation, the initial conditions corresponds to the propagating shock.